NANO LETTERS

pubs.acs.org/NanoLett Letter

Signature of Many-Body Localization of Phonons in Strongly Disordered Superlattices

Thanh Nguyen, Nina Andrejevic, Hoi Chun Po, Qichen Song, Yoichiro Tsurimaki, Nathan C. Drucker, Ahmet Alatas, Esen E. Alp, Bogdan M. Leu, Alessandro Cunsolo, Yong Q. Cai, Lijun Wu, Joseph A. Garlow, Yimei Zhu, Hong Lu, Arthur C. Gossard, Alexander A. Puretzky, David B. Geohegan, Shengxi Huang,* and Mingda Li*

Cite This: *Nano Lett.* 2021, 21, 7419−7425 Read Online

ABSTRACT: Many-body localization (MBL) has attracted significant attention because of its immunity to thermalization, role in logarithmic entanglement entropy growth, and opportunities to reach exotic quantum orders. However, experimental realization of MBL in solid-state systems has remained challenging. Here, we report evidence of a possible phonon MBL phase in disordered GaAs/AlAs superlattices. Through grazing-incidence inelastic X-ray scattering, we observe a strong deviation of the phonon population from equilibrium in samples doped with ErAs nanodots at low temperature, signaling a departure from thermalization. This behavior occurs within finite phonon energy and wavevector windows, suggesting a localization-thermalization crossover. We support our observation by proposing a theoretical model for the effective phonon Hamiltonian in disordered superlattices, and showing that it can be mapped exactly to a disordered 1D Bose−Hubbard model with a known MBL phase. Our work provides momentum-resolved experimental evidence of phonon localization, extending the scope of MBL to disordered solid-state systems.

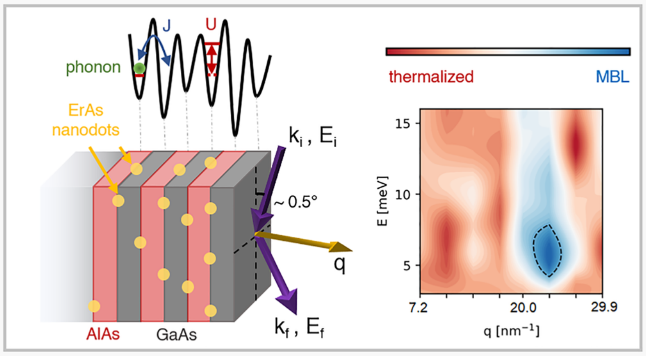

KEYWORDS: *many-body localization, X-ray scattering, phonon, superlattice, Bose-Hubbard model*

Many-body localized (MBL) states subject to strong disorder and strong interactions provide a platform for highly unusual phenomenology.[1−5] Notable examples include the absence of thermalization upon evolution under intrinsic dynamics for parametrically long time scales, quantum phase transitions at nonzero temperatures, and novel dynamical phases of matter. In particular, MBL can protect exotic quantum orders through localization of excitations that would otherwise result in trivialization of the phases.[6−8] Hence, these systems have recently seen heightened interest by serving as a possible pathway toward quantum information processing in systems driven far from equilibrium. MBL has been the subject of exciting studies in well-controlled artificial quantum systems such as ultracold atoms,[9−13] trapped ions,[14] interacting spin chains,[15] and superconducting circuits.[16,17] In contrast to such isolated systems, the unavoidable environmental couplings in a solid-state system smear the sharp features of MBL[18] and thus often preclude further experimental explorations.

In parallel with MBL, the importance of phonon localization can hardly be overlooked. It is well-known that interference between multiple wave scattering paths in systems with even arbitrarily weak disorder can result in Anderson localization depending on the system dimensionality.[19−21] As a fundamental wave phenomenon, Anderson localization has been theoretically studied in a wide variety of systems,[22−27] including phonons.[28−30] However, unlike photons[31−35] and classical waves[36] where coherence can be readily maintained, direct measurements of phonon localization had eluded experiments until recently. The observation of coherent phonons in semiconducting superlattice (SL) systems enabled the exploration of phonon-related phenomena that relied on such coherence.[37] Numerical calculations[38−40] alongside experimental evidence in heat conduction[41] established localization as a fundamental mode of phonon transport.

Nevertheless, open questions remain. Theoretical predictions suggest that phonon localization would transpire within a finite energy interval characterized by multiple mobility edges separating propagating from localized states,[29,38] but momen-

Received: May 17, 2021
Revised: July 14, 2021
Published: July 27, 2021

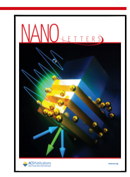

https://doi.org/10.1021/acs.nanolett.1c01905
Nano Lett. 2021, 21, 7419−7425

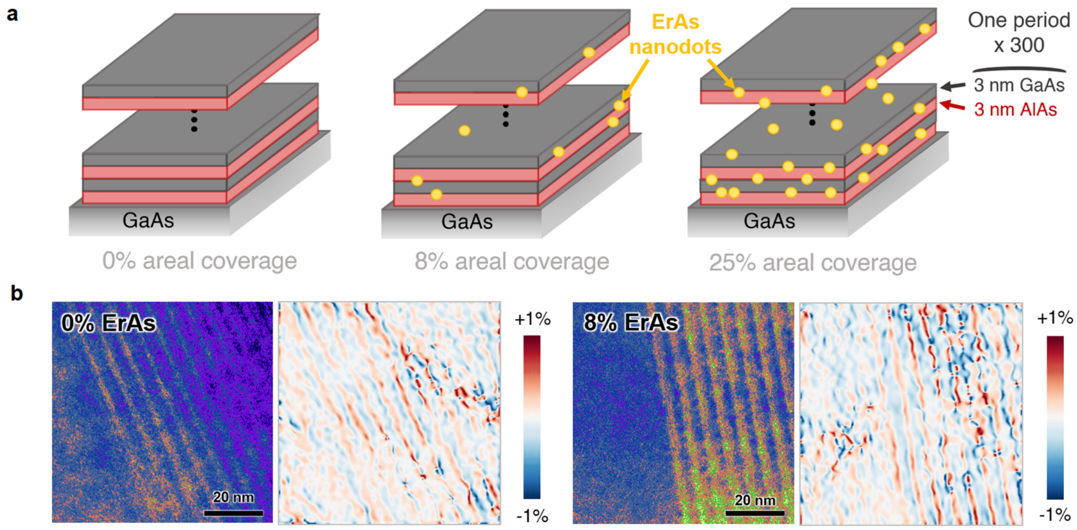

Figure 1. GaAs/AlAs SL samples. (a) Illustration of the pristine ref (0%) and disordered GaAs/AlAs SL samples with 3 nm diameter ErAs nanodots (8% and 25% areal coverage). The SLs consist of 300 periods of 3 nm thick GaAs and 3 nm thick AlAs layers grown on a GaAs substrate. (b) Transmission electron micrograph and related strain mapping of the ref (left two images) and 8% ErAs disordered SLs (right two images).

tum-resolved phonon localization is yet to be demonstrated. The strong interactions and strong disorders in phononic SL systems further call for an MBL description of phonon localization. The elucidation of phonon localization through the lens of MBL would have major implications for connecting the MBL phenomenology to a mesoscopic solid-state system and can shed light on further avenues toward thermoelectric energy conversion and thermal management in microelectronics.[42]

In this work, we experimentally demonstrate a strong departure from phonon thermalization in disordered GaAs/AlAs SLs embedded with ErAs nanodots using grazing-incidence inelastic X-ray scattering (GI-IXS), which reveals a possible manifestation of MBL. Such measurements are technically challenging as they require resolving energy shifts on the order of meV with ∼10 keV X-rays scattered off a micrometer-thick thin film.[43] Comparison of the phonon Stokes and anti-Stokes signals reveals persistent nonequilibrium conditions of the phonon population when disordered ErAs nanodots are introduced. This is suggestive of an MBL phase, which is characterized by an effective temperature that deviates from its thermal value in a canonical ensemble.[44−47] This anomalous behavior occurs systematically within a range of phonon energies and wavevectors at low temperature, revealing a crossover behavior of MBL. We support our experimental results through an exact theoretical mapping between an effective phonon Hamiltonian for disordered SLs and the 1D Bose−Hubbard model with a known MBL phase. Our work presents strongly disordered SL systems as a promising setting to further explore MBL phenomena in solid-state systems.

Sample Characterization. The samples in the GI-IXS experiments comprise three sets of 300-period GaAs/AlAs SLs epitaxially grown on a GaAs (001) substrate. They possess a superperiodicity of 6 nm consisting of a 3 nm GaAs layer followed by a 3 nm AlAs layer. Two disordered SLs are embedded with randomly distributed 3 nm diameter ErAs nanodots: one with an areal density of 8% and the other with 25% (Figure 1a). The average ErAs interparticle distance is 9.5 and 5.5 nm, respectively. The third, pristine SL with 0% nanodot density is kept as a reference (hereafter referred to as "ref"). All samples were grown by molecular beam epitaxy (MBE) in a Veeco Gen III MBE system. The submonolayer ErAs deposition was inserted at the SL interfaces, and the formation of nanodots is caused by the self-assembly of deposited atoms. The size of the ErAs nanodots and the internanodot distances are comparable to the SL superperiodicity, indicating a strong effect of ErAs disorder, in contrast to point-like impurities. Transmission electron microscope-based strain mapping (Figure 1b) shows a low and uniform strain distribution across the SLs, indicating high-quality growth of disordered-SL at a similar strain level of ref-SL. Further characterizations of these samples can be found in the literature.[41]

Nonspecular GI-IXS experiments were carried out at beamline 3-ID-C at the Advanced Photon Source at Argonne National Lab.[48−51] A schematic is illustrated in Figure 2a. With an incident X-ray energy of E_i = 21.7 keV, a grazing incident angle of θ_i = 0.5° was chosen such that the corresponding probing depths λ_a(GaAs) = 0.46 μm and λ_a(AlAs) = 0.82 μm are comparable to the 1.8 μm total SL thickness. This indicates a dominant scattering contribution from the SL rather than from the substrate. Given the large E_i (corresponding to a wavevector k_i = 110 nm^{-1}) and small θ_i, the X-ray wavevector transfer $q \equiv k_i - k_f$ is largely in the out-of-plane direction of the SL in the measured range up to 29.9 nm^{-1}, indicating quasi-1D phonon measurements (calculated phonon dispersions and Raman measurements in the Supporting Information). Constant-q scans of the energy transfer ($E \equiv E_i - E_f$) were performed for all samples at eight different q values, of which three representative ones at low, medium, and high values are shown in Figure 2b (other values in Figure S1). These measurements were performed at an optimized low temperature of 30 K to balance between the long phonon coherence length and the high phonon population,[38] and at room temperature.

At low-q values (q = 10.5 nm^{-1} in Figure 2b), the spectra of the ref SL and disordered SLs behave similarly by nearly overlapping each other. The low phonon and high elastic peak intensities make it difficult to quantitatively extract the phonon

https://doi.org/10.1021/acs.nanolett.1c01905
Nano Lett. 2021, 21, 7419−7425

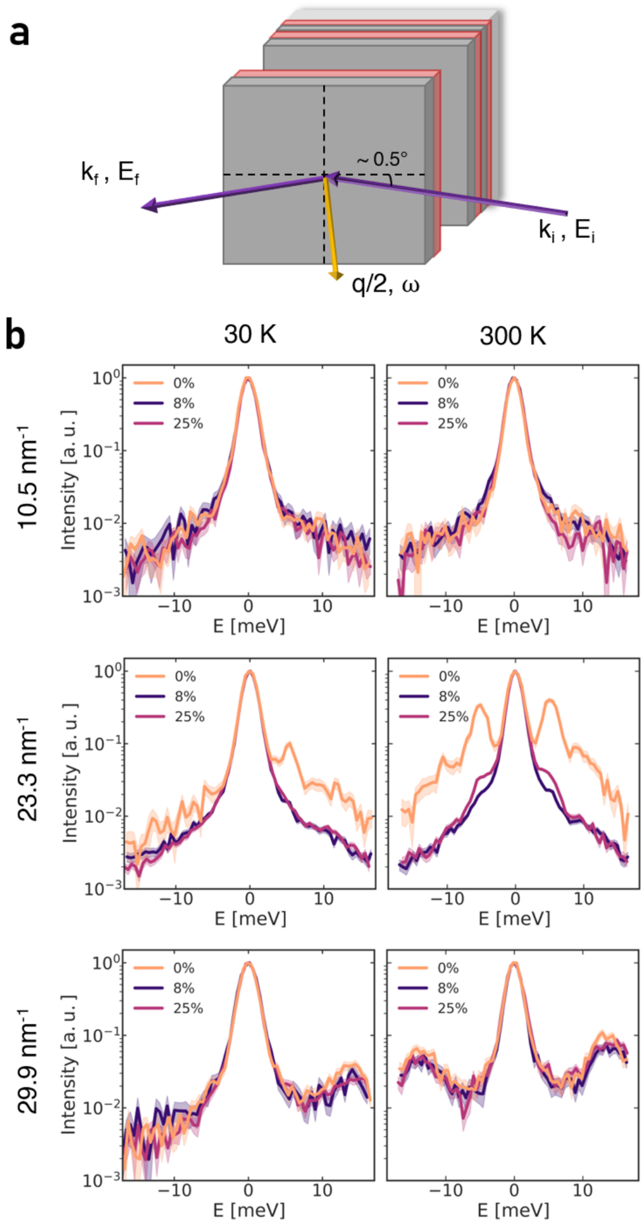

Figure 2. GI-IXS of the GaAs/AlAs SLs. (a) Scattering geometry of the synchrotron-based GI-IXS on the SLs. (b) Comparison of constant-q scans of samples with 0, 8, and 25% ErAs nanodot density at representative q values at 30 K (left column) and 300 K (right column). At medium-q regime near q = 23.3 nm^{-1}, there is a noticeable departure of the phonon spectra between the disordered SLs and the ref-SL. Most importantly, the intensity ratio between the Stokes and the anti-Stokes peaks show anomalous behavior in disordered samples at low temperature. The intensity is normalized and shaded pale regions indicate one standard deviation.

dispersion in this SL system. As one accesses medium-q values (q = 23.3 nm^{-1} in Figure 2b), the behavior of the anti-Stokes (E < 0) and Stokes (E > 0) peaks becomes highly unusual. Thermodynamic equilibrium dictates that the Stokes/anti-Stokes amplitude ratio satisfies detailed balance, where at high temperatures, this ratio approaches unity, and at low temperatures, the Stokes peak intensity dominates over that of the anti-Stokes signal. All samples, regardless of ErAs content, follow this tendency at low-q and high-q regimes for both temperatures. However, two key discrepancies are discernible in the medium-q range. First, whereas the ref SL sample shows significantly larger Stokes peak intensity at low temperature, the disordered SL samples have surprisingly comparable intensities for both anti-Stokes and Stokes peaks at low temperature, highlighting a departure from thermal equilibrium. An attribution to the exciton resonance effect[52] is easily excluded because of the distinct energy scale and temperature profile, and all measured SLs are electrically insulating with no exciton effects. Second, the presence of disorder drastically decreases phonon intensities relative to the elastic peak, indicating a suppressed phonon population.[53] This behavior is most prominent at q = 23.3 nm^{-1} but can also be found in nearby q values. This would point toward delimiting a finite regime of wavevectors where the phonons do not properly thermalize. Moreover, the phonon spectra at q = 23.3 nm^{-1} and low temperature have a broad line width, indicating a high relaxation rate, which further suggests a strong phonon interaction that may facilitate the MBL formation. At high-q values (q = 29.9 nm^{-1} in Figure 2b), the spectra between the ref SL and disordered SLs largely overlap again. A small energy shift between the ref SL and disordered SLs is observed, which may be attributed to the effect of disorder on the phonon energy. All of these conclusions so far can be drawn from raw data prior to further data analysis.

Observation of Localization-Thermalization Crossover. To reinforce the aforementioned claims, we quantify the difference in behavior of the Stokes and the anti-Stokes peak intensities between the ref and disordered samples. The ratio R = I(Stokes)/I(anti-Stokes) for each sample is determined from the GI-IXS spectra as a function of the phonon energy for each constant-q scan, where I is the intensity. The calculation of R is performed without removing the elastic peak to preclude any undesirable artifacts that could arise from elastic-peak subtraction (further analysis in the Supporting Information). The phonons in the ref SL follow equilibrium statistics based on previous evidence.[37] The data are presented to display energy ranges outside those which may be significantly impinged by the elastic peak. To characterize the phonon population imbalance of the disordered samples, we define an imbalance parameter, similar to other studies,[54,55] as

$$\mathcal{I} = \frac{R_{\mathrm{Disorder}} - R_{\mathrm{Ref}}}{R_{\mathrm{Disorder}} + R_{\mathrm{Ref}}} \tag{1}$$

where R_{ref} refers to the ref SL and R_{Disorder} refers to disordered SLs with either 8 or 25% disorder density by area coverage. Plots of this parameter in energy-wavevector space for both disordered samples are shown in Figure 3. Both display $|\mathcal{I}| < 0.15$ at all measured energies and wavevectors at room temperature, where localization is not expected due to strong temperature effects toward equilibrium. Additionally, the GaAs substrate does not have an effect on the measured value of $\mathcal{I}$ (Supporting Information).

As noted from the GI-IXS spectra, the largest imbalance in the phonon population occurs near q = 23.3 nm^{-1} (line cut with error bars in Figure S2), reaching absolute values up to $|\mathcal{I}| \sim 0.5$. This value is comparable to analogous number imbalance measurements within the MBL phase in ultracold atom experiments.[10,11] The SL with lower disorder density (8%) appears to experience a slightly larger imbalance in a more prominent region in energy-wavevector phase space, but the general trend between the two disordered samples is very

https://doi.org/10.1021/acs.nanolett.1c01905
Nano Lett. 2021, 21, 7419−7425

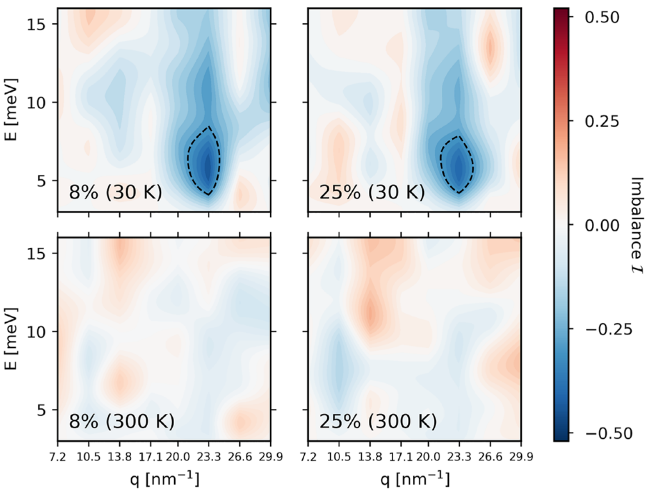

Figure 3. Phonon population imbalance in energy and wavevector parameter space. Phonon population imbalance $\mathcal{I}$ for ErAs-disordered SLs (8%, left column, and 25%, right column) as defined in eq 1. The imbalance is extracted using the data in Figure 2. The high imbalance $\mathcal{I}$ is observed only at low temperature (top row) but not at room temperature (bottom row), whereas the two disordered SLs show large imbalance up to $|\mathcal{I}| \sim 0.5$ in a similar energy window near $E = 6$ meV and wavevector window $q = 23$ nm^{-1}. The dashed lines denote the contour for $|\mathcal{I}| = 0.3$.

similar. Moreover, in addition to the population imbalance taking place within a medium-q window, the behavior also occurs in a finite energy interval between ~4−13 meV. Figure 3 shows distinct regimes in the energy-wavevector phase space with large (dark blue) or weak (light colors) imbalance, which may further serve as a boundary between MBL and thermal phases. As the phononic SL system on a substrate is more akin to an open quantum system, one expects a crossover behavior instead of a sharp transition between the thermal and the MBL phases as in a closed quantum system. Nevertheless, the suppression of phonon population at medium-q regime is indicative of a possible reduction in the effective dimensionality of the site-Hilbert space, which could be a manifestation of a strong local repulsion (Figure 2b).

Effective Phonon Action in Disordered SLs. To gain further insight on the phonon behavior, we develop a minimal model for the phonon transport in the disordered quasi-1D SL system using a tight-binding description. The suitability of the tight-binding approach can be justified as the computed minimum localization length of ~20 nm in disordered SL samples[41] is comparable to the characteristic length scale of the SL system with a superperiodicity of 6 nm. The tight-binding phonon Hamiltonian of the ref SL can be written as

$$H_0 = \sum_i \varepsilon_i n_i + \sum_i t_i (a_{i+1}^\dagger a_i + a_i^\dagger a_{i+1}) \tag{2}$$

where ε_i is the on-site energy of the ith SL layer, $n_i = a_i^\dagger a_i$ is the local phonon population, and t_i is the hopping amplitude between the neighboring SL layers. We further introduce the disorder-field Hamiltonian H_d and the phonon-disorder interaction Hamiltonian H_I as

$$H_\mathrm{d} = \frac{1}{2}\sum_i \varepsilon_{\mathrm{d},i}\xi_i^2$$
$$H_\mathrm{I} = \sum_i g_i a_i^\dagger a_i \xi_i, \tag{3}$$

where $\varepsilon_{\mathrm{d},i} > 0$ is the on-site disorder energy of the ith SL layer, ξ_i is the disorder field, and g_i is the local phonon-disorder coupling strength. The on-site disorder energy $\varepsilon_{\mathrm{d},i}$ is appropriate because of the mass difference by the ErAs nanodots. The phonon-disorder coupling is proportional to the phonon population n_i, which is also reasonable.

For a comprehensive impurity average calculation, either replica theory,[56,57] Keldysh formalism,[58] or supersymmetry method[59] should be implemented. Here for a qualitative estimate without loss of generality, we define the effective phonon action S_eff by integrating over the disorder degrees of freedom:

$$e^{-S_\mathrm{eff}} = e^{-S_0}\int D\xi e^{-S_\mathrm{d}[\xi]-S_\mathrm{I}[\xi]} \tag{4}$$

where $D\xi = \prod_i d\xi_i$ is the functional measure. Such treatment makes the disorder field resemble annealed disorder. By carrying out an explicit calculation of eq 4, and further defining that $J = -t_i$, $U_i = g_i^2/\varepsilon_{\mathrm{d},i}$, $\mu_i = \varepsilon_i + g_i^2/(2\varepsilon_{\mathrm{d},i})$, we obtain the 1D Bose−Hubbard model

$$H_\mathrm{BH} = \sum_i \mu_i n_i - J\sum_i (a_{i+1}^\dagger a_i + a_i^\dagger a_{i+1}) + \frac{1}{2}\sum_i U_i(n_i^2 - n_i) \tag{5}$$

This model has been extensively studied and shown to exhibit an MBL phase.[60,61] Furthermore, the MBL in this model is characterized by an *inverted* mobility edge in which higher energy states are localized,[62,63] similar to what is observed in our GI-IXS experiment.

The on-site repulsion U_i in eq 5 is an important parameter controlling the model behavior, and can be estimated as (see the Supporting Information)

$$U_i \propto \frac{R^2}{N n_\mathrm{B}(\varepsilon_{\mathrm{d},i})}\sqrt{\frac{m_\mathrm{Er}}{m_\mathrm{eff}}} \tag{6}$$

where R is the nanodot radius, n_B is the Bose−Einstein distribution, m_Er is the mass of Er atom from disorders, m_eff is the effective mass from Al and Ga atoms from ref SLs, and N denotes the system size. A number of experimental features can be reconciled with eq 6. First, the disorder concentration η is canceled out and absent in eq 6, which is consistent with the similar behavior observed in our 8 and 25% samples in the parameter regime with large phonon population imbalance. Second, the large mass differences between Er atoms and the Ga and Al atoms tend to increase U_i and favor MBL. Third, the large disorder radius R with an R^2-dependence also facilitates a large U_i. Lastly, a lower phonon population inside the disorder $n_\mathrm{B}(\varepsilon_{\mathrm{d},i})$ can generate a larger U_i, which agrees with the observation that at medium-q phonon population is suppressed, whereas imbalance $\mathcal{I}$ is high. The possibility to exactly map the strongly disordered quasi-1D phonon transport into the Bose−Hubbard model, as well as the guideline to increase on-site repulsion using eq 6, hints at a new avenue to seek MBL in disordered SL solid-state systems.

https://doi.org/10.1021/acs.nanolett.1c01905
Nano Lett. 2021, 21, 7419−7425

Discussion. In our SL system, the natural choice of system size is the total period of SL $N = 300$. However, coherent phonon behavior can be observed in an $N = 16$ SL,[37] within which the inter-SL transport can be "coarse-grained" as one effective site. In accordance with the long phonon coherence and long phonon mean-free-path l_{MFP} in an SL with total thickness L,[38] the effective system size for a $N = 300$ period SL gives $N_{eff} = N\, l_{MFP}/L < 20$, which serves the role of N in eq 6 and further increases the on-site repulsion. In addition, the observed imbalance $\mathcal{I}$ takes on an extreme value near $E = 5$ meV, with $\mathcal{I} = -0.5$, whereas it diminishes to $\mathcal{I} = -0.15$ near $E = 15$ meV, indicating the existence of two mobility edges in energy. Although the 1D Bose−Hubbard model has only one inverted mobility edge, the additional mobility edge can be intuitively understood as resulting from high-energy extended modes which can be added to eq 2 as longer-range hopping terms. This behavior qualitatively agrees with the self-consistent diagrammatic theory of phonon localization in hard-sphere scatterers,[29] and semiquantitatively with the nonequilibrium Green's function calculations in this SL system showing the localization regime at around 6 to 10 meV.[38] On the other hand, the localization window in wavevector space has not been predicted since theories either integrate over momentum degrees of freedom or set the momentum to zero for simplicity.[28,29] In our 6 nm superperiodic SL, $q \approx 20$ nm^{-1} corresponds to an ∼40-fold extended Brillouin zone. From the computed SL phonon dispersion,[41] this enters into the phonon energy at $E \approx 10$ meV, above the lower-energy delocalized regime. Consequently, the localization window in wavevector space may naturally be linked to the localization window in energy space.

Conclusion. In summary, we provide momentum-resolved evidence of signatures of many-body localization in disordered semiconducting phononic SLs, through state-of-the-art low temperature GI-IXS measurements. The disordered SL platform contains the essential elements that can lead to the realization of MBL: a reduced dimensionality that limits the pathways to drive the system toward thermal equilibrium, while the nanodot-type disorder with size comparable to the SL spacing can provide strong on-site interaction and strong disorder effects. By investigating the quasiparticle population imbalance, we uncover that phonons in the disordered SL samples fail to thermalize within finite energy and wavevector windows. This likening of the experimental observations to the MBL phenomenology is further supported by theoretical calculations showing the equivalence between the quasi-1D tight-binding phonon transport under strong disorder and the 1D Bose−Hubbard model with a known MBL phase. In particular, our experimental findings qualitatively agree with the criteria to reach high on-site repulsion that favors an MBL phase. Our study opens up new opportunities in two directions: as a new experimental solid-state platform for realizing possible MBL phenomena, and as a novel phonon phase far away from equilibrium.

■ ASSOCIATED CONTENT

Supporting Information

The Supporting Information is available free of charge at https://pubs.acs.org/doi/10.1021/acs.nanolett.1c01905.

Parameter estimation of the strong Hubbard interaction, data analysis of GI-IXS measurements, phonon dispersion of GaAs/AlAs/ErAs superlattices, effect of GaAs substrate, and Raman scattering (PDF)

■ AUTHOR INFORMATION

Corresponding Authors

Mingda Li − *Department of Nuclear Science and Engineering, Massachusetts Institute of Technology, Cambridge, Massachusetts 02139, United States;* orcid.org/0000-0002-7055-6368; Email: mingda@mit.edu

Shengxi Huang − *Department of Electrical Engineering, The Pennsylvania State University, University Park, Pennsylvania 16802, United States;* orcid.org/0000-0002-3618-9074; Email: sjh5899@psu.edu

Authors

Thanh Nguyen − *Department of Nuclear Science and Engineering, Massachusetts Institute of Technology, Cambridge, Massachusetts 02139, United States*

Nina Andrejevic − *Department of Material Science and Engineering, Massachusetts Institute of Technology, Cambridge, Massachusetts 02139, United States*

Hoi Chun Po − *Department of Physics, Massachusetts Institute of Technology, Cambridge, Massachusetts 02139, United States*

Qichen Song − *Department of Mechanical Engineering, Massachusetts Institute of Technology, Cambridge, Massachusetts 02139, United States*

Yoichiro Tsurimaki − *Department of Mechanical Engineering, Massachusetts Institute of Technology, Cambridge, Massachusetts 02139, United States*

Nathan C. Drucker − *John A. Paulson School of Engineering and Applied Sciences, Harvard University, Cambridge, Massachusetts 02138, United States*

Ahmet Alatas − *Advanced Photon Source, Argonne National Laboratory, Lemont, Illinois 60439, United States;* orcid.org/0000-0001-6521-856X

Esen E. Alp − *Advanced Photon Source, Argonne National Laboratory, Lemont, Illinois 60439, United States*

Bogdan M. Leu − *Advanced Photon Source, Argonne National Laboratory, Lemont, Illinois 60439, United States; Department of Physics, Miami University, Oxford, Ohio 45056, United States*

Alessandro Cunsolo − *Department of Physics, University of Wisconsin at Madison, Madison, Wisconsin 53706, United States*

Yong Q. Cai − *National Synchrotron Light Source II, Brookhaven National Laboratory, Upton, New York 11973, United States*

Lijun Wu − *Condensed Matter Physics and Material Science Department, Brookhaven National Laboratory, Upton, New York 11973, United States*

Joseph A. Garlow − *Condensed Matter Physics and Material Science Department, Brookhaven National Laboratory, Upton, New York 11973, United States*

Yimei Zhu − *Condensed Matter Physics and Material Science Department, Brookhaven National Laboratory, Upton, New York 11973, United States;* orcid.org/0000-0002-1638-7217

Hong Lu − *College of Engineering and Applied Sciences, Nanjing University, Nanjing, China;* orcid.org/0000-0002-8340-2739

https://doi.org/10.1021/acs.nanolett.1c01905
Nano Lett. 2021, 21, 7419−7425

Arthur C. Gossard − *Materials Department, University of California, Santa Barbara, Santa Barbara, California 93106, United States*

Alexander A. Puretzky − *Center for Nanophase Materials Sciences, Oak Ridge National Laboratory, Oak Ridge, Tennessee 37831, United States;* orcid.org/0000-0002-9996-4429

David B. Geohegan − *Center for Nanophase Materials Sciences, Oak Ridge National Laboratory, Oak Ridge, Tennessee 37831, United States;* orcid.org/0000-0003-0273-3139

Complete contact information is available at: https://pubs.acs.org/10.1021/acs.nanolett.1c01905

Notes

The authors declare no competing financial interest.

■ ACKNOWLEDGMENTS

The authors thank R. Nandkishore and P. Cappellaro for helpful discussions. T.N., N.A., N.C.D., and M.L. acknowledge the support from U.S. Department of Energy (DOE), Office of Science, Basic Energy Sciences (BES), award DE-SC0020148. N.A. acknowledges the support of the National Science Foundation Graduate Research Fellowship Program under Grant 1122374. M.L. acknowledges support from Norman C. Rasmussen Career Development Chair. S.H. acknowledges the support from the National Science Foundation under grant number ECCS-1943895. H.C.P. is supported by a Pappalardo Fellowship at MIT and a Croucher Foundation Fellowship. Work of Q.S. and Y.T. was supported by Solid State Solar-Thermal Energy Conversion Center (S3TEC), an Energy Frontier Research Center funded by the U.S. Department of Energy, Office of Science, Basic Energy Sciences, award DE-SC0001299 (prior to January 2019). Y.Q.C., L.W., J.G., and Y.Z. acknowledge the support from DOE/BES, the Materials Science and Engineering Divisions, under Contract DE-SC0012704. This research used resources of the Advanced Photon Source, a U.S. DOE Office of Science User Facility operated for the DOE Office of Science by Argonne National Laboratory, under Contract DE-AC02-06CH11357. Raman measurements were conducted at the Center for Nanophase Materials Sciences (CNMS), which is a DOE Office of Science User Facility.

■ REFERENCES

(1) Basko, D. M.; Aleiner, I. L.; Altshuler, B. L. Metal-insulator transition in a weakly interacting many-electron system with localized single-particle states. *Ann. Phys.* **2006**, *321*, 1126−1205.

(2) Pal, A.; Huse, D. A. Many-body localization phase transition. *Phys. Rev. B: Condens. Matter Mater. Phys.* **2010**, *82*, 174411.

(3) Nandkishore, R.; Huse, D. A. Many-Body Localization and Thermalization in Quantum Statistical Mechanics. *Annu. Rev. Condens. Matter Phys.* **2015**, *6*, 15−38.

(4) Abanin, D. A.; Altman, E.; Bloch, I.; Serbyn, M. Colloquium: Many-body localization, thermalization, and entanglement. *Rev. Mod. Phys.* **2019**, *91*, 021001.

(5) Khemani, V.; Hermele, M.; Nandkishore, R. Localization from Hilbert space shattering: From theory to physical realizations. *Phys. Rev. B: Condens. Matter Mater. Phys.* **2020**, *101*, 174204.

(6) Huse, D. A.; Nandkishore, R.; Oganesyan, V.; Pal, A.; Sondhi, S. L. Localization-protected quantum order. *Phys. Rev. B: Condens. Matter Mater. Phys.* **2013**, *88*, 014206.

(7) Chandran, A.; Khemani, V.; Laumann, C. R.; Sondhi, S. L. Many-body localization and symmetry-protected topological order. *Phys. Rev. B: Condens. Matter Mater. Phys.* **2014**, *89*, 144201.

(8) Pekker, D.; Refael, G.; Altman, E.; Demler, E.; Oganesyan, V. Hilbert-Glass Transition: New Universality of Temperature-Tuned Many-Body Dynamical Quantum Criticality. *Phys. Rev. X* **2014**, *4*, 011052.

(9) Kondov, S.; McGehee, W.; Xu, W.; DeMarco, B. Disorder-Induced Localization in a Strongly Correlated Atomic Hubbard Gas. *Phys. Rev. Lett.* **2015**, *114*, 083002.

(10) Schreiber, M.; Hodgman, S. S.; Bordia, P.; Lüschen, H. P.; Fischer, M. H.; Vosk, R.; Altman, E.; Schneider, U.; Bloch, I. Observation of many-body localization of interacting fermions in a quasirandom optical lattice. *Science* **2015**, *349*, 842−845.

(11) Choi, J. Y.; Hild, S.; Zeiher, J.; Schauß, P.; Rubio-Abadal, A.; Yefsah, T.; Khemani, V.; Huse, D. A.; Bloch, I.; Gross, C. Exploring the many-body localization transition in two dimensions. *Science* **2016**, *352*, 1547−1552.

(12) Lukin, A.; Rispoli, M.; Schittko, R.; Tai, M. E.; Kaufman, A. M.; Choi, S.; Khemani, V.; Léonard, J.; Greiner, M. Probing entanglement in a many-body-localized system. *Science* **2019**, *364*, 256−260.

(13) Rispoli, M.; Lukin, A.; Schittko, R.; Kim, S.; Tai, M. E.; Léonard, J.; Greiner, M. Quantum critical behaviour at the many-body localization transition. *Nature* **2019**, *573*, 385−389.

(14) Smith, J.; Lee, A.; Richerme, P.; Neyenhuis, B.; Hess, P. W.; Hauke, P.; Heyl, M.; Huse, D. A.; Monroe, C. Many-body localization in a quantum simulator with programmable random disorder. *Nat. Phys.* **2016**, *12*, 907−911.

(15) Wei, K. X.; Ramanathan, C.; Cappellaro, P. Exploring Localization in Nuclear Spin Chains. *Phys. Rev. Lett.* **2018**, *120*, 070501.

(16) Roushan, P.; Neill, C.; Tangpanitanon, J.; Bastidas, V. M.; Megrant, A.; Barends, R.; Chen, Y.; Chen, Z.; Chiaro, B.; Dunsworth, A.; Fowler, A.; Foxen, B.; Giustina, M.; Jeffrey, E.; Kelly, J.; Lucero, E.; Mutus, J.; Neeley, M.; Quintana, C.; Sank, D.; Vainsencher, A.; Wenner, J.; White, T.; Neven, H.; Angelakis, D. G.; Martinis, J. Spectroscopic signatures of localization with interacting photons in superconducting qubits. *Science* **2017**, *358*, 1175−1179.

(17) Xu, K.; Chen, J.-J.; Zeng, Y.; Zhang, Y.-R.; Song, C.; Liu, W.; Guo, Q.; Zhang, P.; Xu, D.; Deng, H.; Huang, K.; Wang, H.; Zhu, X.; Zheng, D.; Fan, H. Emulating Many-Body Localization with a Superconducting Quantum Processor. *Phys. Rev. Lett.* **2018**, *120*, 050507.

(18) Nandkishore, R.; Gopalakrishnan, S. Many body localized systems weakly coupled to baths. *Ann. Phys.* **2017**, *529*, 1600181.

(19) Anderson, P. W. Absence of Diffusion in Certain Random Lattices. *Phys. Rev.* **1958**, *109*, 1492−1505.

(20) Abrahams, E.; Anderson, P. W.; Licciardello, D. C.; Ramakrishnan, T. V. Scaling Theory of Localization: Absence of Quantum Diffusion in Two Dimensions. *Phys. Rev. Lett.* **1979**, *42*, 673−676.

(21) Lee, P. A.; Ramakrishnan, T. V. Disordered electronic systems. *Rev. Mod. Phys.* **1985**, *57*, 287−337.

(22) Cutler, M.; Mott, N. F. Observation of Anderson Localization in an Electron Gas. *Phys. Rev.* **1969**, *181*, 1336−1340.

(23) Thouless, D. J. Electrons in disordered systems and the theory of localization. *Phys. Rep.* **1974**, *13*, 93−142.

(24) Sutherland, B. Localization of electronic wave functions due to local topology. *Phys. Rev. B: Condens. Matter Mater. Phys.* **1986**, *34*, 5208−5211.

(25) John, S. Strong localization of photons in certain disordered dielectric superlattices. *Phys. Rev. Lett.* **1987**, *58*, 2486−2489.

(26) Weaver, R. L. Anderson localization of ultrasound. *Wave Motion* **1990**, *12*, 129−142.

(27) Sanchez-Palencia, L.; Clément, D.; Lugan, P.; Bouyer, P.; Shlyapnikov, G. V.; Aspect, A. Anderson Localization of Expanding Bose−Einstein Condensates in Random Potentials. *Phys. Rev. Lett.* **2007**, *98*, 210401.

(28) John, S.; Sompolinsky, H.; Stephen, M. J. Localization in a disordered elastic medium near two dimensions. *Phys. Rev. B: Condens. Matter Mater. Phys.* **1983**, *27*, 5592−5603.
(29) Kirkpatrick, T. R. Localization of acoustic waves. *Phys. Rev. B: Condens. Matter Mater. Phys.* **1985**, *31*, 5746−5755.
(30) Sheng, P.; Zhou, M.; Zhang, Z.-Q. Phonon transport in strong-scattering media. *Phys. Rev. Lett.* **1994**, *72*, 234−237.
(31) Albada, M. P. V.; Lagendijk, A. Observation of Weak Localization of Light in a Random Medium. *Phys. Rev. Lett.* **1985**, *55*, 2692−2695.
(32) Wolf, P.-E.; Maret, G. Weak Localization and Coherent Backscattering of Photons in Disordered Media. *Phys. Rev. Lett.* **1985**, *55*, 2696−2699.
(33) Wiersma, D. S.; Bartolini, P.; Lagendijk, A.; Righini, R. Localization of light in a disordered medium. *Nature* **1997**, *390*, 671−673.
(34) Schwartz, T.; Bartal, G.; Fishman, S.; Segev, M. Transport and Anderson localization in disordered two-dimensional photonic lattices. *Nature* **2007**, *446*, 52−55.
(35) Segev, M.; Silberberg, Y.; Christodoulides, D. N. Anderson localization of light. *Nat. Photonics* **2013**, *7*, 197−204.
(36) Hu, H.; Strybulevych, A.; Page, J. H.; Skipetrov, S. E.; van Tiggelen, B. A. Localization of ultrasound in a three-dimensional elastic network. *Nat. Phys.* **2008**, *4*, 945−948.
(37) Luckyanova, M. N.; Garg, J.; Esfarjani, K.; Jandl, A.; Bulsara, M. T.; Schmidt, A. J.; Minnich, A. J.; Chen, S.; Dresselhaus, M. S.; Ren, Z.; Fitzgerald, E. A.; Chen, G. Coherent Phonon Heat Conduction in Superlattices. *Science* **2012**, *338*, 936−939.
(38) Mendoza, J.; Chen, G. Anderson Localization of Thermal Phonons Leads to a Thermal Conductivity Maximum. *Nano Lett.* **2016**, *16*, 7616−7620.
(39) Hu, S.; Zhang, Z.; Jiang, P.; Chen, J.; Volz, S.; Nomura, M.; Li, B. Randomness-Induced Phonon Localization in Graphene Heat Conduction. *J. Phys. Chem. Lett.* **2018**, *9*, 3959−3968.
(40) Juntunen, T.; Vänskä, O.; Tittonen, I. Anderson Localization Quenches Thermal Transport in Aperiodic Superlattices. *Phys. Rev. Lett.* **2019**, *122*, 105901.
(41) Luckyanova, M. N.; Mendoza, J.; Lu, H.; Song, B.; Huang, S.; Zhou, J.; Li, M.; Dong, Y.; Zhou, H.; Garlow, J.; Wu, L.; Kirby, B. J.; Grutter, A. J.; Puretzky, A. A.; Zhu, Y.; Dresselhaus, M. S.; Gossard, A.; Chen, G. Dresselhaus, A. Gossard, and G. Chen, Phonon localization in heat conduction. *Sci. Adv.* **2018**, *4*, eaat9460.
(42) Maldovan, M. Sound and heat revolutions in phononics. *Nature* **2013**, *503*, 209−217.
(43) Serrano, J.; Bosak, A.; Krisch, M.; Manjón, F. J.; Romero, A. H.; Garro, N.; Wang, X.; Yoshikawa, A.; Kuball, M. InN Thin Film Lattice Dynamics by Grazing Incidence Inelastic X-Ray Scattering. *Phys. Rev. Lett.* **2011**, *106*, 205501.
(44) Rossini, D.; Silva, A.; Mussardo, G.; Santoro, G. E. Effective Thermal Dynamics Following a Quantum Quench in a Spin Chain. *Phys. Rev. Lett.* **2009**, *102*, 127204.
(45) Canovi, E.; Rossini, D.; Fazio, R.; Santoro, G. E.; Silva, A. Many-body localization and thermalization in the full probability distribution function of observables. *New J. Phys.* **2012**, *14*, 095020.
(46) Lenarčič, Z.; Altman, E.; Rosch, A. Activating Many-Body Localization in Solids by Driving with Light. *Phys. Rev. Lett.* **2018**, *121*, 267603.
(47) Lenarčič, Z.; Alberton, O.; Rosch, A.; Altman, E. Critical Behavior near the Many-Body Localization Transition in Driven Open Systems. *Phys. Rev. Lett.* **2020**, *125*, 116601.
(48) Sinn, H.; Alp, E.; Alatas, A.; Barraza, J.; Bortel, G.; Burkel, E.; Shu, D.; Sturhahn, W.; Sutter, J.; Toellner, T.; Zhao, J. An inelastic X-ray spectrometer with 2.2meV energy resolution. *Nucl. Instrum. Methods Phys. Res., Sect. A* **2001**, *467−468*, 1545−1548.
(49) Alatas, A.; Leu, B.; Zhao, J.; Yavas, H.; Toellner, T.; Alp, E. Improved focusing capability for inelastic X-ray spectrometer at 3-ID of the APS: A combination of toroidal and Kirkpatrick-Baez (KB) mirrors. *Nucl. Instrum. Methods Phys. Res., Sect. A* **2011**, *649*, 166−168.
(50) Toellner, T. S.; Alatas, A.; Said, A. H. Six-reflection meV-monochromator for synchrotron radiation. *J. Synchrotron Radiat.* **2011**, *18*, 605−611.
(51) Sinn, H. Spectroscopy with meV energy resolution. *J. Phys.: Condens. Matter* **2001**, *13*, 7525−7537.
(52) Goldstein, T.; Chen, S.-Y.; Tong, J.; Xiao, D.; Ramasubramaniam, A.; Yan, J. Raman scattering and anomalous Stokes-anti-Stokes ratio in $MoTe_2$ atomic layers. *Sci. Rep.* **2016**, *6*, 1−7.
(53) De Francesco, A.; Scaccia, L.; Maccarini, M.; Formisano, F.; Zhang, Y.; Gang, O.; Nykypanchuk, D.; Said, A. H.; Leu, B. M.; Alatas, A.; Cai, Y. Q.; Cunsolo, A. Damping Off Terahertz Sound Modes of a Liquid upon Immersion of Nanoparticles. *ACS Nano* **2018**, *12*, 8867−8874.
(54) Levi, E.; Heyl, M.; Lesanovsky, I.; Garrahan, J. P. Robustness of Many-Body Localization in the Presence of Dissipation. *Phys. Rev. Lett.* **2016**, *116*, 237203.
(55) Lüschen, H. P.; Bordia, P.; Hodgman, S. S.; Schreiber, M.; Sarkar, S.; Daley, A. J.; Fischer, M. H.; Altman, E.; Bloch, I.; Schneider, U. Signatures of Many-Body Localization in a Controlled Open Quantum System. *Phys. Rev. X* **2017**, *7*, 011034.
(56) Mezard, M.; Parisi, G.; Virasoro, M. A. *Spin Glass Theory and Beyond: An Introduction To The Replica Method and Its Applications*; World Scientific: Singapore, 1987; pp 7−384.
(57) Dotsenko, V. *Introduction to the Replica Theory of Disordered Statistical Systems*; Cambridge University Press: New York, 2001; pp 13−212.
(58) Kamenev, A. *Field Theory of Non-Equilibrium Systems*; Cambridge University Press, 2011; pp 210−297.
(59) Efetov, K. Supersymmetry and theory of disordered metals. *Adv. Phys.* **1983**, *32*, 53−127.
(60) Michal, V.; Altshuler, B.; Shlyapnikov, G. Delocalization of Weakly Interacting Bosons in a 1D Quasiperiodic Potential. *Phys. Rev. Lett.* **2014**, *113*, 045304.
(61) Michal, V. P.; Aleiner, I. L.; Altshuler, B. L.; Shlyapnikov, G. V. Finite-temperature fluid−insulator transition of strongly interacting 1D disordered bosons. *Proc. Natl. Acad. Sci. U. S. A.* **2016**, *113*, E4455−E4459.
(62) Sierant, P.; Delande, D.; Zakrzewski, J. Many-body localization due to random interactions. *Phys. Rev. A: At., Mol., Opt. Phys.* **2017**, *95*, 021601.
(63) Sierant, P.; Zakrzewski, J. Many-body localization of bosons in optical lattices. *New J. Phys.* **2018**, *20*, 043032.

https://doi.org/10.1021/acs.nanolett.1c01905
Nano Lett. 2021, 21, 7419−7425